

# Geological object aligned PEBI grids and fracture modelling: A comparative analysis and enhancements

Shahid Manzoor<sup>1\*</sup>, Raheel Ahmed<sup>1</sup> and Tareq Al Shaalan<sup>1</sup>

<sup>1</sup>Strategic Modelling Technology, Saudi Aramco, Core Area, Dhahran, 31311, Eastern Province, Saudi Arabia.

\*Corresponding author(s). E-mail(s): [shahid.manzoor.1@aramco.com](mailto:shahid.manzoor.1@aramco.com);

## Abstract

We present methods for generating geological objects aligned unstructured PEBI grids. Using these grids, we perform a sensitivity analysis of fractured reservoirs in which fractures are represented either as embedded lower-dimensional features or as explicitly gridded entities of equal or reduced dimensionality. We compare the performance of fracture-modelling approaches. In the embedded discrete fracture model (EDFM), fractures are represented as lower-dimensional cells connected to surrounding matrix cells through non-neighbour connections. From a grid-generation perspective, fracture networks are inserted after the matrix grid is built, requiring the computation of fracture-matrix intersections. We generate a range of grids with varying refinement levels around fractures to demonstrate the capabilities of the PEBI grid generator. Numerical results from EDFM are benchmarked against a discrete fracture modelling (DFM) approach, which relies on more complex PEBI grids aligned to fractures with respect to control points and/or volumes. For DFM, the fracture network is honoured first, followed by meshing of the surrounding domain. Simulation results show that pressure-transient behaviour near fractures is better captured when smooth local refinement is used. However, compared to DFM, EDFM does not require that fracture cells be aligned with matrix, and nor does it enforce continuity of flux. Consequently, EDFM cannot accurately resolve flow across low-permeability barriers. We also test EDFM on advanced control-point-aligned and locally refined PEBI grids. Although some improvement in flow resolution is observed, EDFM still fails to capture flow around barriers. To address this limitation, we propose a modification for barrier cases: thereby assigning harmonic mean of matrix and fracture permeabilities to matrix cells associated with non-neighbour connections. Numerical experiments show that updating the permeabilities of these

underlying matrix cells enables EDFM to reproduce flow behaviour around barriers comparable to that of DFM.

**Keywords:** Meshing, PEBI-Grids, Fracture Modelling, Discrete-Fracture, EDFM, Finite-Volume, TPFA

## 1 Introduction

Fractures are a system of rock discontinuities, e.g., faults, joints and fissures, that occur in porous media with apertures having widths ranging over scales from microns to centimetres [1]. Open fractures act as preferential fluid flow paths above a certain aperture and size whereas cemented fractures can act as flow barriers. Flow, in any rock, is affected by a few large fractures, by a dense network of small fractures, or by a combination of fractures of varying length scales ranging from microns to hundreds of kilometres [2, 3]. Usually the matrix provides the storage for the fluid while fractures provide the main fluid flow paths. For example, in two-phase flow, fractures may form the predominant flow paths for a particular phase and the less permeable matrix may become the flow region for the other phase [4]. There is an immense importance in energy production and environmental problems for understanding of fluid flow through a fractured porous medium. The oil industry has a special interest because an estimated 60% of the world's remaining oil reserves reside in fractured formations [5]. In addition to oil and gas production fracture modelling is of interest in determining carbon sequestration strategies, radioactive waste management in the subsurface [6], and flow of non-aqueous-phase liquids in aquifers.

Fractured reservoirs are characterized by the presence of two distinct types of porous media: matrix and fracture [7]. The matrix and fractured media have very different fluid storage and conductivity characteristics. The importance of fractures in reservoirs has led to increasing effort being devoted to development of efficient and accurate numerical methods to simulate fluid flow through fractured porous media. Dual-porosity/permeability models, developed in [8–11], have traditionally been used for the last few decades. Flow transfer terms are defined between the fracture and matrix systems. These transfer terms depend on the shape factor, average pressure difference between two domains and further physical parameters in the case of multi-phase flow [12]. The shape factor is not straightforward to determine and is not available in the presence of capillarity and gravity for two-phase flow [6]. Barriers cannot be modelled by dual-porosity/permeability models. Moreover, these models are based on assumption that fracture systems are dense so inaccurate results are produced for large scale fractures. As a result, the discrete-fracture model (DFM) was developed; see e.g., [6, 13–26], which is attractive for large scale and sparse fracture systems. In this model actual geometry and location of the fracture are honoured in the domain. Unlike the dual-porosity model; the effect of individual fractures on fluid flow can be determined and fluid transfer between the fracture and matrix is straightforward and consistent. Generally, fractures are modelled by  $(n - 1)$  dimensional elements in an  $n$ -dimensional domain, for example in 2D, fractures are represented by lines at

the edges of the polygonal matrix elements. Equidimensional representation of fractures [27], are not popular because of complexity and computational cost contributed by thin cells. In the equidimensional model, the control-volume at the intersection of the fractures is of the dimensions of fracture aperture which reduces the time step size in the numerical model [6]. Also, in our experience with this method we have observed that a small control-volume increases the condition number of the global linear system which increases the computational cost for the solution of the system, consistent with [28].

In equidimensional discrete-fracture method, rock-matrix and fracture elements coincide at the interface (conforming DFM), so an unstructured grid is used to honour the explicit fracture geometry, e.g., [29, 30]. Also, the matrix cells near the fracture are small enough to conform to the fracture geometry. Small cells lead to a large numerical system to be solved. Because of grid conformity, this model may not be applied to dynamic fracture network modelling where the grid is updated because of generation of new fractures [31, p. 72]. Moreover, the discrete-fracture model may not be used for small scale fractures and any cases with large numbers of fractures, which would lead to locally dense unstructured grids in-turn leading to high computational cost. A hybrid method (fracture-only model) that gets advantages of both dual-porosity method and discrete-fracture method has been presented in [32]. Hierarchical fracture models have been presented in [16] for flow simulation in a fractured porous medium. In this approach, small scale fractures are homogenized into the matrix medium and their effects are added to the matrix permeability. Large scale fractures are explicitly modelled as major fluid conduits embedded in non-conforming structured meshes, the approach known as embedded discrete fracture model (EDFM) [33]. Conforming unstructured meshes capture heterogeneity of a porous medium precisely and give better resolution near fractures, in particular, for multiphase flow. While embedded discrete fracture model provides the flexibility of using the structured meshes [34]. A comparison of conforming DFM, EDFM and dual-porosity model can be found in [35].

Here, we present dual-cell (PEBI) feature preserved Delaunay admissible grid generation methods and assess performance of different fracture modelling techniques [36]. Note that grids are generated by employing simplexes (primal-cells) and PEBI (dual) cells are selected as control volumes, consequently fractures are meshed with respect to (dual) control volumes. We begin with development of fracture based PEBI grid generation techniques, which can be employed to generate quality meshes for reservoir geometries. For lower/equidimensional fracture modelling, methods to generate boundary aligned grids are described. In contrast, EDFM does not require boundary aligned grids, instead involves fractures and matrix intersection with non-neighbour connections. In order to construct control-point aligned grids we use protection circles build around key geological features, this ensures integrity of features in the final Delaunay triangulation. The idea of protection-circles is unique and does not impair the PEBI property associated with Delaunay meshes. For dual-cell control volume aligned grids, it is a prerequisite to build a (protection) layer of quadrilaterals, with a geological feature defining the median line inside the quadrilateral layer, we call this additional protection layer a halo. A halo protected primal mesh is essentially Delaunay and honours geological features with respect to dual-cells. Next using industry

standard two-point flux approximation numerical results are presented, and comparative performance of fracture modelling approaches is assessed. For EDFM performance is also assessed by employing control point aligned grids, i.e., comparative studies with fractures aligned along the centroids of the grid cells versus the randomly intersecting fractures away from the centroids are also presented.

## 2 PEBI gridding and fracture modelling

Subsurface reservoirs are often comprised of complex geometric and geologic objects and features. In addition to robust numerical methods for solving the flow equations, grid generation methods are required which can honour geometric complexity and permit local grid cell density control. Grid generation for large scale porous media poses the challenge of complex geometries and random distribution of spatial heterogeneities in the domain, e.g., [18, 37]. Standard reservoir simulators were originally based on simple grid blocks, i.e., squares and cubes primarily using structured grids. Although it is relatively easy to implement simulation techniques on such simple grids, they inherently lack the ability to adapt to general geological features and complex geometries [38]. Unstructured grid generation offers the desired flexibility by employing triangles and tetrahedra as grid elements. Unstructured grids allow grid cells to adapt to various flow and geometric constraints and also local refinement with smooth transition [39]. Despite unstructured grid generation methods having been successfully employed in modelling complex giant reservoirs, in field applications there is still increased inclination toward the use of structured grids. This might be the result of novelty of these methods in the field compared with structured grids for which well-established simulation tools exist, and consequently more research work is required for simulation on unstructured grids.

The unstructured grids used in reservoir modelling, commonly employ Delaunay (PEBI) grids for spatial discretization of domain. Delaunay triangulation (DT) is the dual of the Voronoi (power) diagram [40], given a DT grid, the dual can be constructed. *Voronoi* based grids are locally orthogonal, and permit two-point flux approximation if the permeability field is isotropic, or if the grid is generated to be K-orthogonal[41]. *Voronoi* grids are also called Dirichlet or Thiessen tessellations. Mathematically, each *voronoi* region  $v_i$ , associated with a site  $s_i$  is defined by:

$$v_i = \{p \mid d(p, s_i) \leq d(p, s_j), \forall j \neq i\} \quad (1)$$

where  $d(p, s_i)$  is the Euclidean distance between a point  $p$  belonging to  $v_i$  and associated site  $s_i$ . The boundary between two sites  $s_1$  and  $s_2$ , also called a *voronoi* edge, and is a line segment given by points( $p$ ) which satisfy  $d(p, s_1) = d(p, s_2)$ . Delaunay triangulations lead to the construction of PEBI (PERpendicular BIssectional) grids, e.g., see Figure 1c. From the grid generation view point it is relatively easy to work with Delaunay triangulation directly, and dual grids are obtained as the circumcentre or centroid dual of the associated Delaunay triangulation. A triangulation is Delaunay if no simplex circumcircle contains any site in its interior. Figure 1 shows a simple example of Delaunay triangulation and associated dual grid, constructed by joining circumcentres



of cells having an edge adjacency. In order to ensure that the circumcircle of every simplex is empty Delaunay triangulation relies on the Delaunay measure [42].

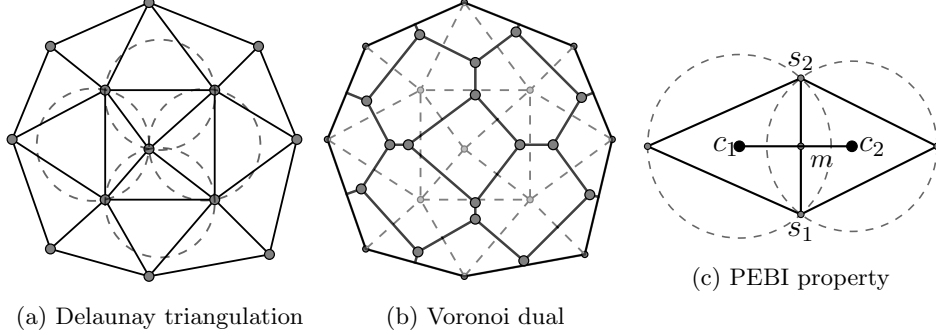


**Fig. 1:** Delaunay Triangulation (DT) satisfy empty circumcircle criterion, and corresponding circumcentre dual (Voronoi) of underlying Delaunay triangulation

## 2.1 Fracture based PEBI grid generation

Key components involved in fracture based PEBI grid generation are displayed in a flow chart given in Fig. 2. In what follows these steps are briefly described, more detail can be found elsewhere [36].

### *Boundary discretization, curve modelling, and curve meshing*

To start with triangulation internal and external boundaries defining geometry of the reservoir, wells-trajectories, definition of faults/fractures, pinch-outs, and/or layers are first discretized with desired resolution. For domain and interior boundaries set of control points having both geometric, i.e., coordinates, and metric support are assumed as input. Each boundary is modelled as a set of B-Spline curves and can be input in control or interpolation design with least number of points. The interior boundaries are modelled using cubic spline, and curve meshing is performed in metric space generating a data set where each line segment is of unit metric length [43]. In order to demonstrate the procedure devised to mesh boundaries, in the following we mesh an air-foil. The control polygons for a B-spline curve defining air-foil geometry, both in control and interpolation design [44] are displayed in Fig. 3a. In Fig. 3a the blue circles correspond to the control points (B), whereas the red circles are their associated data points (S), and underlying black curve is the B-Spline curve, obtained by constructing the Bezier curve between each set of two consecutive data points. Each B-Spline curve is then approximated as a polygonal line, e.g., see Fig. 3b & 3c. Note that the control points have metrics defining density function. To generate a governed triangulation operating on each arc one-one we compute the metric length of each arc. In Fig. 3d metric length of an arc between points A and B has been subdivided into 14 sub-segments where each sub-segment is of unit metric length. The unit metric

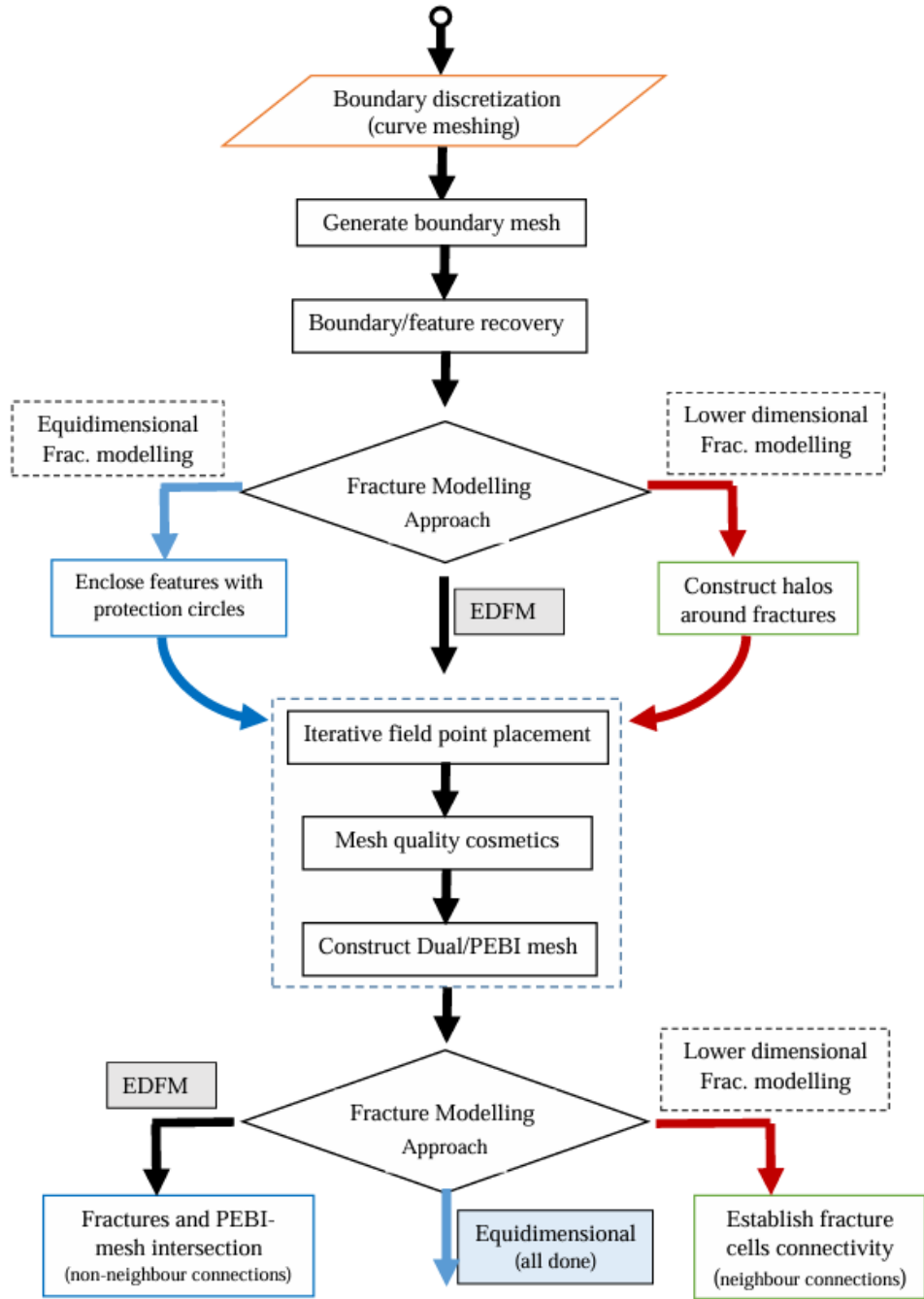


**Fig. 2:** Flow chart highlighting key steps involved in fracture based PEBI grid generation method

length mesh in metric space, when mapped to physical space, conforms to input metric specification.

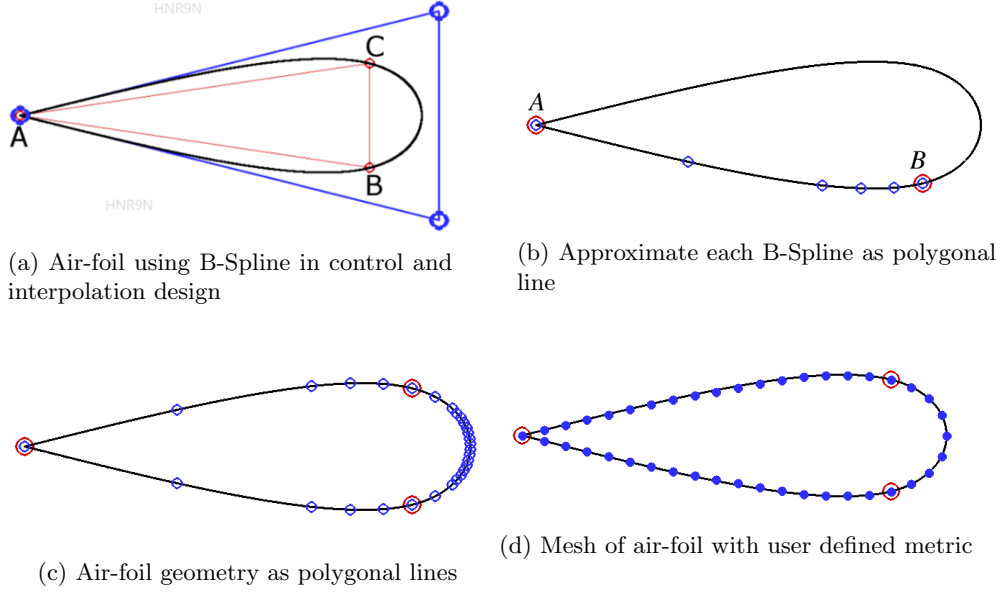


**Fig. 3:** Curve modelling, approximating curve as polygonal line, and curve meshing

### *Boundary meshing and feature recovery*

To start with any triangulation, a prerequisite is to construct an empty (boundary) mesh, comprised of a prescribed set of points defining domain boundaries and/or geological features. We use the Green-Sibson algorithm [45] in conjunction with the incircle criterion for connection optimization, which yields the Delaunay empty mesh of a predefined set of points, e.g., see Fig. 4a. Delaunay triangulation is the triangulation of a convex hull of a predefined data set. In a Delaunay triangulation connection are improved such that none of the simplexes contains any site in its interior, but it cannot be guaranteed that connections between the given point set are present in a prescribed/desired manner [46]. Thus, to recover interior/exterior boundaries it is mandatory to couple the Delaunay triangulation algorithm with a boundary (feature) recovery technique. In what follows we briefly outline two commonly employed methods including local refinement [46] also called the stitching method, and edge swapping [47] used to constrain the mesh to honour a feature. Consider a simple Delaunay triangulation shown in Fig. 4a, where an edge  $ab$  defining feature is missing. The local refinement technique requires new points introduced midway between each missing connection, recursively, until the desired edge is recovered. . On the other hand edge swapping involves swapping edges intersected by the segment  $ab$  recursively until the feature is recovered. Figs. 4b & 4c are pictorial representations of

field edge  $ab$  constrained triangulations, achieved through local refinement and edge swapping respectively. It can be noticed that the former of these boundary recovery approaches results in the conformal Delaunay triangulation, i.e., PEBI-Grid, while the later yields a non-conformal Delaunay triangulation (essentially Delaunay). In this work we employ the local refinement to recover missing boundaries, and/or features in the boundary/empty mesh, which are then preserved throughout the field mesh generation process described below.

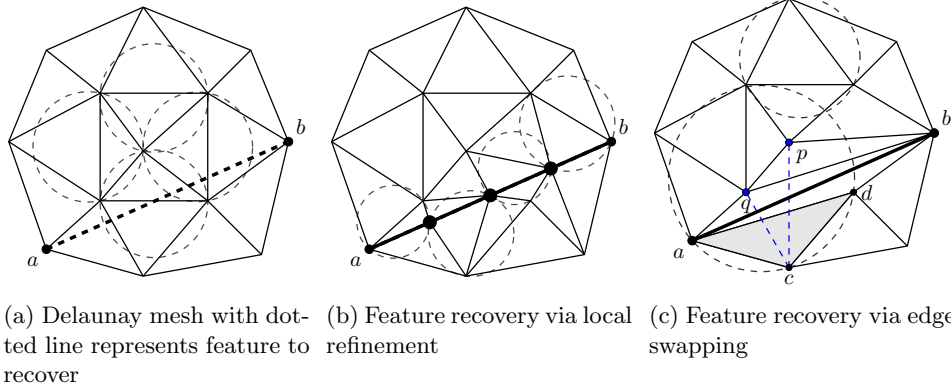
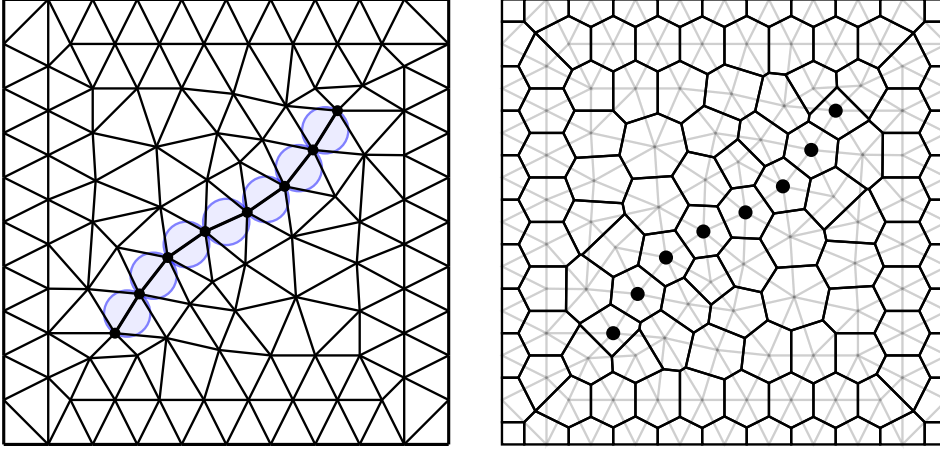


**Fig. 4:** Honouring a feature via local refinement (conformal DT) and through edge swapping (non-conformal DT) technique.

#### *Protect features and/or halo construction*

For equidimensional and/or lower dimensional fracture modelling approaches this step is required, e.g., Fig. 3. In contrast, for EDFM fractures are meshed in a post-processing step. For equidimensional fracture modelling approach fracture cells are equidimensional (dual) control-volumes with small size defined by fracture-aperture. Here, curves defining fractures are first recovered in boundary meshing stage. The feature aligned Delaunay empty/boundary mesh comprises of low-quality elements. In order to generate a well resolved mesh comprised of quality simplexes, the empty mesh is refined by introducing new (field) points, and/or mesh cosmetics (smoothing algorithms) are applied. The Delaunay triangulation of new field points encroaching simplexes honouring geological features can lead to reconfiguration of these connections, destroying boundary integrity. In order to avoid swapping and to preserve integrity of features honoured in the empty mesh, we construct protection circles that pass through the simplexes constituting geological features. The protection circle used is either diametric or a simplex-circle. In field mesh generation integrity of features is maintained provided new points encroaching the protection circles are not accepted. Also, when applying any mesh cosmetics, the edges defining geological objects are not swapped. More details about protection circle can be found in [36]. Starting with an empty mesh, a field triangulation is carried out, such that the Delaunay property of

edges defining geological features is preserved. To this end edges constituting features are marked as Delaunay admissible edges and are protected by constructing protection circles around them. Fig. 5 (left) displays a test case feature honoured mesh, with protection circles drawn around the edges constituting the feature. Note that these disks were drawn around simplexes constituting features to be honoured in the empty-mesh, and defines a region where no field point is accepted. The empty mesh was refined by introducing new points in an iterative manner. The final primal-cell feature honoured mesh is displayed in Fig. 5 (left). The dual of feature protected primal mesh has control volumes with their cell-centres (control-points) aligned to the fractures. Note that for illustration purpose only, Fig. 5 assumes that fracture and matrix cells are of same size.

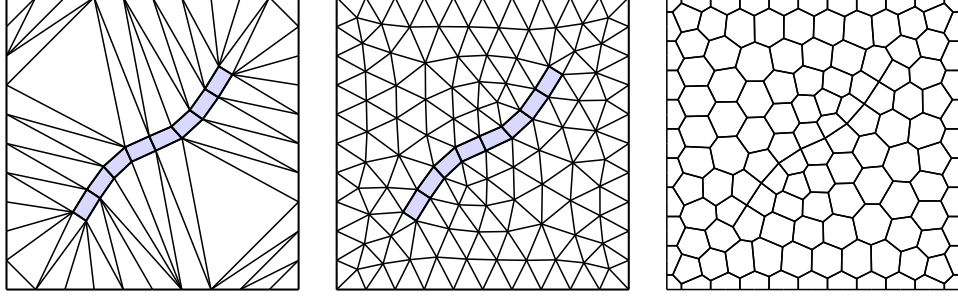


(a) Geological feature enclosed with protection circles (b) Dual cell control-point aligned PEBI grid

**Fig. 5:** Procedure to generate equi-dimensional fracture aligned PEBI mesh

For lower-dimensional fracture modelling, in final dual mesh, fracture control volumes are lower dimensional, i.e., one-dimensional, and recovered as control volume interfaces. PEBI control-volumes are generated such that their boundaries honour geological objects, control-volume faces crossing the fractures are not allowed. In order to generate dual mesh where (dual) matrix cells interfaces are aligned with lower-dimensional fracture cells, in the primal empty/boundary mesh, geological objects are first enclosed by a protection layer, i.e., quadrilateral halos. Note that protection layer is added around fractures in primal triangular mesh and encloses fractures as medial curve. In dual setting this would ensure that geological object is honoured/recovered as control volume boundaries. Detailed description of halo construction can be found in [36]. For lower-dimensional fracture simulation, first reservoir domain and interior

boundaries are triangulated and missing features are recovered. Next fractures are protected by enclosing them with halos as shown in Fig. 6 (left). Field mesh generation is performed without impairing connectivity of halo quads. To this end the edges constituting halo quads are constraints, and during field mesh generation any new (field) point falling inside halo quads is not accepted. Furthermore, for field meshing, we use advancing front point placement which initiates fronts from these quad edges, providing protection around halo quad edges. The resulting halo protected feature based primal grid is shown in Fig. 6 (middle), and due to halo elements is essentially Delaunay. The dual of the halo protected primal-mesh corresponds to dual-cell boundary aligned grids, e.g., see Fig. 6 (right).



(a) Halo-protected boundary mesh (b) Halo protected primal mesh (c) Feature aligned dual mesh

**Fig. 6:** Key steps involved generating lower dimensional fracture aligned PEBI mesh

#### *Field mesh generation, mesh-cosmetics, and dual mesh*

Delaunay is a criterion to connect a predefined set of points, which of course is optimal in many aspects [48, 49]. The boundary/empty mesh constructed from a prescribed boundary discretization comprises of low-quality elements. In order to generate a quality grid, this empty mesh is locally refined by introducing new field points. Several options exist to introduce field (interior) points in an empty mesh, so as to design an automatic Delaunay triangulation algorithm. In general point placement strategies involve introducing field points at either the centroid [50], circumcentre [51], by edge subdivision [52] of the elements in the background mesh. This process of point placement is used repetitively, until the desired edge length or some other criterion measuring element size is satisfied. It is well established that DT has a sound mathematical basis, while its counterpart, the advancing front method provides optimal point placement. In this work we use advancing front point placement [53–56], where field points are introduced in a manner similar to the advancing front method, while their connections are improved by enforcing the Delaunay criterion, and is named as advancing front local reconnection (AFLR) Delaunay triangulation method [54]. The advancing front method used in conjunction with Delaunay criterion both provides

optimal point placement, and makes it relatively easy to generate boundary aligned grids, where integrity of boundaries is a further advantage. Figure 7 displays comparative uniform isotropic mesh of a unit square domain generated with different field point placements. Grids shown in Figure 7 are not subject to any mesh cosmetic.

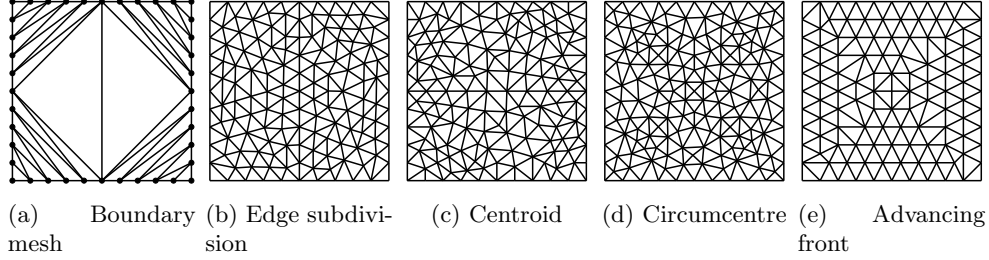


**Fig. 7:** Uniform isotropic mesh of unit square domain, by using different field point placement strategies

Mesh cosmetics can be applied to improve quality of mesh. However, in case there are interior boundaries and/or protection layers edges defining geological objects are not swapped. Here to improve mesh quality we use smoothing algorithm given in [43], and can generate quality circumcentre contained acute triangulations. Note that there is a duality between Delaunay triangulation and Voronoi (powers) diagram given one other can be constructed.

## 2.2 Example Fracture Aligned PEBI-Grids:

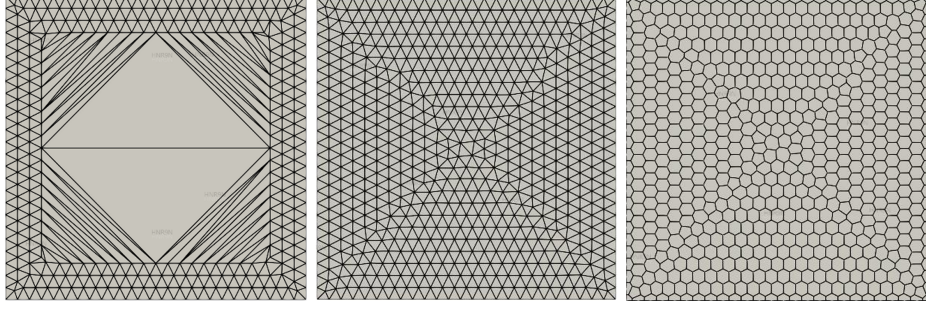
In below, we demonstrate the capabilities of workflow to generate fracture-aligned meshes for different fracture-modelling techniques. We begin by outlining the meshing procedure for the Embedded Discrete Fracture Model (EDFM), where fractures are inserted as lower-dimensional features into an existing matrix grid. We then describe mesh generation for lower-dimensional Discrete Fracture Modelling (DFM), in which fracture geometries are explicitly honoured during grid construction. Finally, we present the workflow for equidimensional DFM, where fractures are fully resolved as volumetric cells.

### *Generating EDFM fracture mesh:*

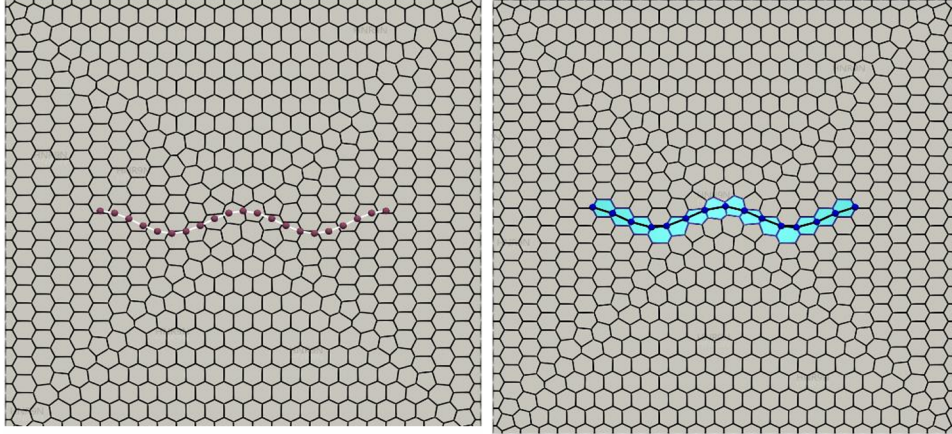
For EDFM, fractures need not to be boundary aligned. Consequently, PEBI grids are generated without interior boundaries (fractures), e.g., Fig. 8a. Fractures are embedded after PEBI grid generation is done with. Method to mesh fractures in unstructured PEBI-grid is described below. Fractures are first discretized, to this end curve modelling is used and fractures are approximated as polygonal straight-line graph (PSLG) as discussed earlier. Figure 8b displays a representative fracture curve approximated as polygonal line. To model fractures EDFM employs non-conformal lower dimensional control-volume and requires to compute intersection of polygonal lines and underlying



polygonal PEBI mesh. From Fig. 8b, it can be noted that data set defining fractures polygonal line are not the intersection points of grid and fractures. Embedding fractures in a PEBI grid is an involved procedure, here each polygonal line is meshed incrementally, i.e., one at a time. First intersection points are computed and then connected in an unstructured manner to generate lower dimensional fracture cells. Since EDFM fracture cells are not boundary aligned with respect PEBI-grid, to model flow between fracture and matrix (PEBI) cells, non-neighbour connections are added. Note that fracture to fracture connections are neighbouring connections. Figure 8c delineate fracture embedded as PEBI mesh intersection points, where highlighted polygonal PEBI cells will have fracture cells as their lower dimensional non-neighbour cells.



(a) Delaunay triangulation and PEBI mesh for EDFM without interior boundaries



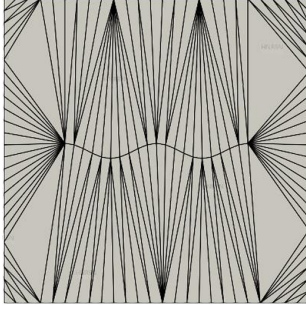
(b) PEBI mesh with a representative fracture approximated as polygonal line (c) PEBI mesh with fracture embedded as grid intersection points

**Fig. 8:** PEBI grid for EDFM, after resolving fractures intersections (embedding), fracture cells are connected to underlying matrix through non-neighbour connections

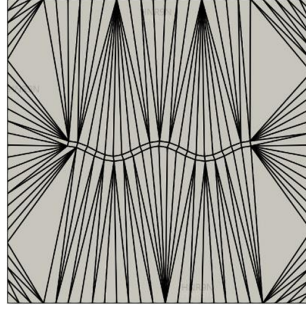


### *Lower dimensional DFM: Halo protected PEBI grid*

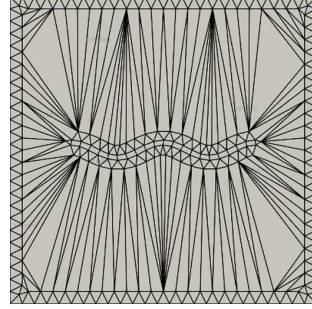
For lower dimensional fracture modelling fractures gridded as lower dimensional geological objects. Mesh generation is performed with respect to primal-cells (triangles/quads), where fractures are enclosed with quadrilateral halos. Figure 9a displays a representative fracture meshed as interior boundary and in Fig. 9b has been enclosed with quad-halo. Next field meshing is performed generating halo protected primal-mesh, e.g., Figs. 9c and 9d. Dual of halo protected primal mesh is boundary (feature) aligned PEBI grid as shown in Fig. 9e. Note that dual cell interfaces are aligned with fractures. These interfaces define lower dimensional control volume and with width given by fracture aperture. Note that lower dimensional fracture cells are by design neighbouring connections to adjacent PEBI grids.



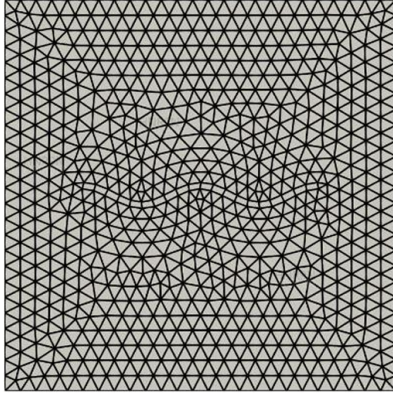
(a) Empty mesh with discrete fracture



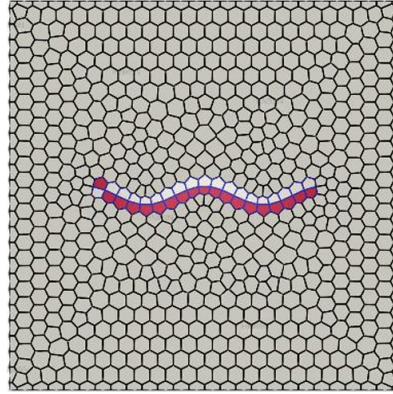
(b) Halo enclosing fracture



(c) Field meshing with AFLR



(d) Halo protected primal mesh



(e) Fracture aligned PEBI-mesh

**Fig. 9:** Halo protected mesh and lower dimensional fracture modelling

### *Equidimensional DFM and control point aligned PEBI grids*

For equidimensional fracture modelling fracture control volume have same dimension as that of matrix control volume. However, fracture cell size is controlled by fracture aperture and compared to matrix is very small. We generate PEBI-grid with smooth transition, consequently matrix cells in the neighbourhood of fractures are also small. Here, fracture cells centroid (i.e., control-points) are aligned with fracture geometry. Grid generation is performed with respect to primal (triangular) cells. In empty mesh fracture curves are meshed and are protected with protection circles. Final primal and dual (PEBI) mesh with local refinement and smooth transition from fracture to matrix is displayed in Fig. 10. In Fig. 10 a close up of resulting PEBI grid is also shown, where fracture cells (highlighted) have centroids (control-points) aligned with the fracture in a close proximity

## 3 Numerical discretization and flux approximation:

The grids generated, provide a means of spatial discretization required by flux approximation schemes. The flux approximation schemes used in reservoir simulation are control volume distributed (CVD), where a piecewise constant representation of flow variables and rock properties is assigned to control volumes, so that field variables are located at their centres, and/or circumcentres also called control points [40]. The grids generated must be compatible with the flux approximation schemes employed. The two-point flux approximation (TPFA) involving a two-point pressure difference to approximate the flux across interfaces of control-volume, and is still regarded as the standard reservoir simulation flux approximation [57]. Here, using TPFA we simulate pressure field and tracer transport, and assess comparative performance of fracture modelling techniques.

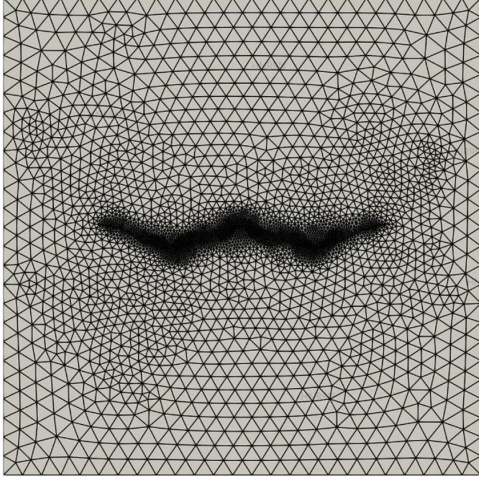
### 3.1 Pressure equation

We compute pressure field by solving the following pressure equation that arises from Darcy's law and mass conservative for single phase flow:

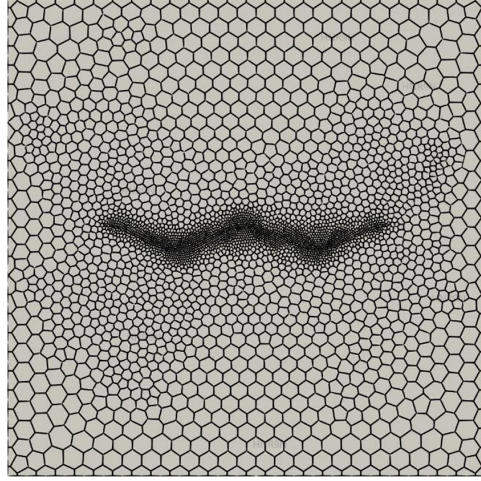
$$-\int_{\Omega} \nabla \cdot (K \nabla P) d\Omega = q \quad (2)$$

where,  $P$  represents field pressure;  $\nabla$  is the gradient operator,  $K$  is the elliptic symmetric permeability tensor;  $q$  is the source term, which is zero away from well sources or sinks. The first step of the finite-volume formulation involves use of the Gauss divergence theorem to integrate Eq. (2), over a control-volume  $\Omega$ . After integration, Eq. (2) is then written as

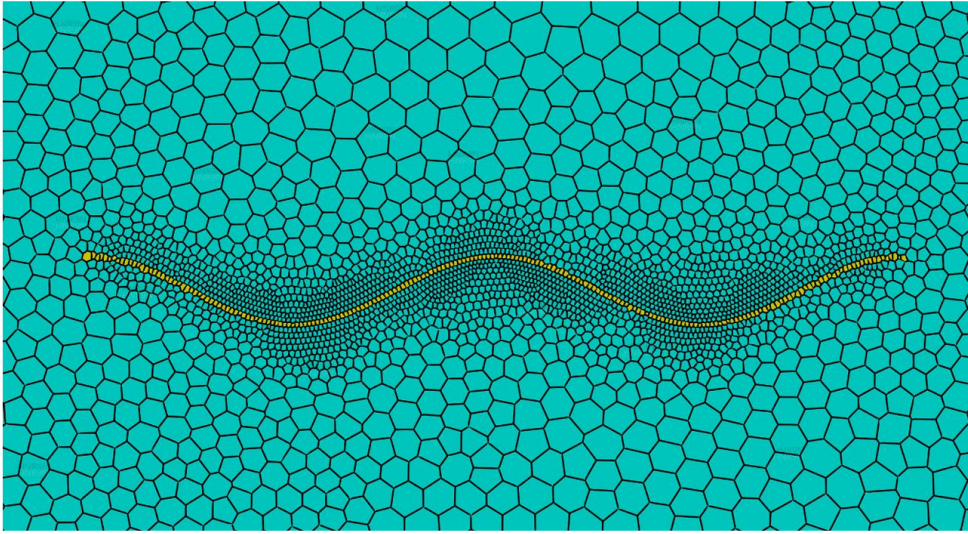
$$-\oint_{\partial\Omega} (K \nabla P) \cdot \vec{n} d\Gamma = -\sum_{i=1}^{n_f} \int_{\Delta\Omega_i} (K \nabla P \cdot \vec{n}_i) d\Gamma = q \quad (3)$$



(a) Fracture boundary aligned primal mesh



(b) Control-point fracture aligned PEBI-Grid



(c) Close up of control-point fracture aligned PEBI-Grid

**Fig. 10:** Control point aligned PEBI grid and equidimensional fracture modelling

where  $\delta\Omega$  corresponds to the boundary of control-volume  $\Omega$ ,  $d\Gamma$  is an element of control-volume surface area,  $\Delta\Omega_i$  is the  $i^{th}$  face of the control-volume and  $n_f$  is the number of faces;  $\vec{n}_i$  is the outward unit normal to face  $i$  as shown in Figure 11. The resolution of Darcy velocity  $-K\nabla P$  along the unit normal  $n_i$  is called the Darcy-flux through face  $i$ . Approximation of Darcy-flux is a key step in a finite-volume formulation and many approximations have been proposed, here we use two-point flux approximation (TPFA) scheme.



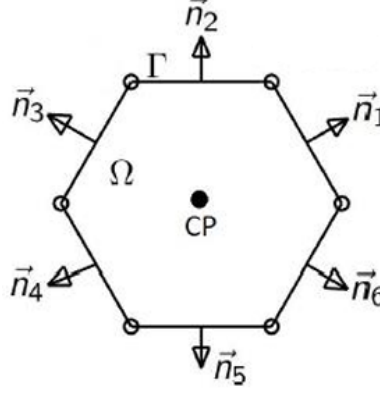


**Fig. 11:** A representative polygonal control volume

### 3.2 Tracer transport equation

The mass conservation equation for tracer transport ignoring dispersion is advection equation [58] given by:

$$\varphi \frac{\partial c}{\partial t} + \nabla \cdot (\vec{v}c) = q \quad (4)$$

where,  $c$  represents the tracer concentration and  $\varphi$  is porosity, here assumed as unity for simplicity. Here,  $\vec{v}$  is the discrete Darcy velocity given by  $-K\nabla P$ , and  $q$  corresponds to a source term which is zero away from wells. The spatial and temporal discretization of Eq. (4) over a representative control volume  $\Omega_i$  (shown in Fig. 11) followed by application of the Gauss divergence theorem yields:

$$\frac{c^{n+1} - c^n}{\Delta t} A_\Omega - \sum_{i=1}^{n_f} (K \nabla P \times c \cdot \vec{n}) = q \times A_\Omega \quad (5)$$

where,  $A_\Omega$  is the size (area) of a control-volume  $\Omega$ .

### 3.3 Conforming (boundary aligned) discrete fracture modelling

In the widely used (lower-dimensional) DFM approach, the fractures are modelled by the interfaces of the grid cells. A fracture-aligned grid is generated where grid cells conform to the discrete-fractures modelled lower-dimensionally. Here, an unstructured grid is generated with special treatment to align the boundary of the grid cells with the fractures keeping the fractures geometry intact, e.g., Fig. 9. Referring to Fig. 12 which displays two representative control volumes and following the two-point flux approximation (TPFA) scheme, the transmissibility between two cells  $T_{12}$  is calculated as:

$$T_{12} = \frac{t_1 t_2}{t_1 + t_2}, \quad \text{where} \quad t_i = \frac{K_i \vec{d}_i \cdot \vec{n}_i A}{\vec{d}_i \cdot \vec{d}_i} \quad i = 1, 2 \quad (6)$$

where,  $K_i$  is the permeability tensor of a cell  $i$ ,  $\vec{d}_i$  is distance vector from the interface centre to the cell centroid,  $A$  is the interface area (length in 2D) and  $\vec{n}_i$  is the normal

vector to the interface. The transmissibility of matrix-matrix cells (matrix neighbour connections) is calculated as mentioned above. If any interface of a matrix cell is a lower dimensional fracture instead of an interface with other matrix cell, fracture-matrix transmissibility is calculated with the fracture half-transmissibility is as follows:

$$t_2 = t_f = \frac{K_f \vec{n} \cdot \vec{n} A}{\frac{a_f}{2}} \quad (7)$$

where,  $a_f$  is the fracture aperture (width). In case of fracture-fracture cells (fracture neighbour connection) the transmissibility is calculated the same way Eq. (6) as mentioned above with  $A = a_f$  and  $\vec{d}_i$  is the distance from the intersection point of fractures to the centre of the fracture cell  $i$ , and  $\vec{n}_i$  is the unit vector of  $\vec{d}_i$ . Details are also given in [18].

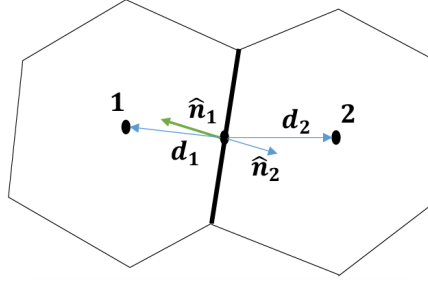


**Fig. 12:** Schematic of two-point flux approximation between two cells

### 3.4 Embedded discrete fracture modelling (EDFM)

As discussed above embedded discrete fracture model does not require any special treatment of the grid that can be aligned. The fractures overlap the grid and can intersect (overlay) the matrix cells at any direction. This approach is attractive for commercial simulators using corner point grids. Any grid cell of matrix that is intersected by a fracture is identified and the fracture is called a non-neighbour connection (NNC) of that matrix cell. A flux transfer is then added to the mass conservation equation of the matrix cell and the intersecting fracture cell. The approximation of the flux transfer is dependent on the geometrical location of the fracture relative to the intersected matrix cell. Further details are given in [34, 59]. The matrix cell to fracture cell transmissibility is calculated as:

$$T_{mf} = \frac{\bar{K} A}{d_{NNC}} \quad (8)$$

where,  $\bar{K}$  is the harmonic mean of the matrix and fracture permeability aligned in the normal direction of the fracture cell:

$$\bar{K} = \frac{K_f K_m}{K_f + K_m} \quad (9)$$

For  $K_f \gg K_m$ ,  $\bar{K} \approx K_m$  as used in [23]. The  $d_{NNC}$  is the volume (area) weighted average of distances of fracture centroid to the centroids of the sub-grid cells (projected to the normal to fracture) of a matrix cell that is intersected by the fracture, illustrated in Fig. 13 (right), and is calculated as:

$$d_{NNC} = \frac{\sum_i |\vec{d}_i \cdot \hat{n}| V_i}{\sum_i V_i} \quad (10)$$

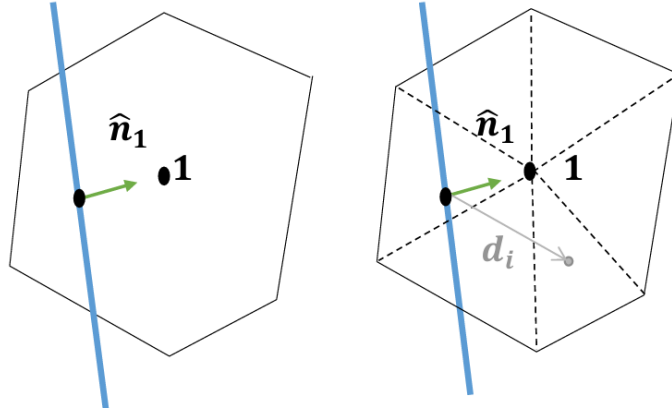


**Fig. 13:** Illustration of embedded discrete fracture model and schematic of the  $d_{NNC}$  calculation (right)

### 3.5 Improved EDFM (for barriers)

In contrast to DFM, in EDFM fracture cells does not lie at the interfaces between fracture/barrier, and matrix; and flux-continuity is not enforced. As a result, EDFM by design is unable to resolve flow field across the barriers. In this work in case of barriers to improve EDFM performance, when resolving Darcy velocity across the interfaces of underlying matrix cells (intersected with fractures/barriers) we propose to use harmonic mean of permeability of matrix and fracture given by Eq (9). Note that permeability of matrix cells tagged with non-neighbour connections is replaced with harmonic mean of matrix and non-neighbour barrier cells permeability. Numerical experiments demonstrate that if permeability of underlying matrix cells is updated by Eq.(9), then EDFM can resolve flow field around the barriers similar to DFM. Here to

improve  $d_{NNC}$  calculations, we also employ control point aligned PEBI grids, where EDFM fractures can be recovered as medial line of underlying matrix cells, with added improvement.

## 4 Numerical results

We present two test cases to compare the fracture models.

### 4.1 Case 1: Single permeable fracture

First, we test single phase pressure and tracer flow simulation on a simple case with a single permeable fracture as shown in Fig. 14. The permeability of the fracture is 10000 times higher than the surrounding matrix and the aperture assumed is 0.001. We dis-

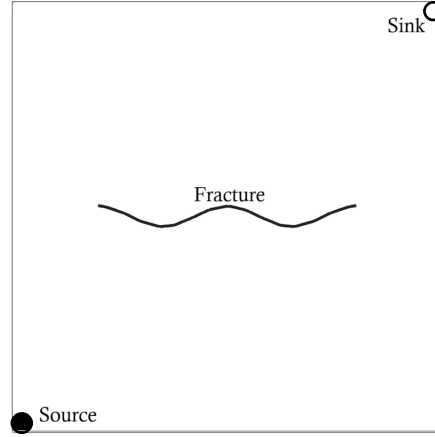


**Fig. 14:** Case-1: A model with a single permeable fracture

cretise the domain with the PEBI cells for: a) DFM model with grid edges aligned with the fractures; b) EDFM where fracture overlaps the grid cells; c) EDFM but grid centroids aligned with fracture; and d) Equidimensional model where a physical fracture is discretised into small grid cells within high resolution grid. PEBI grids used are displayed in Figs. 8,9 and 10. The bottom left corner is a source with high pressure where tracer is injected and the top-right corner is a sink with a low-pressure assignment. To minimize grid orientation effect, we compare EDFM with lower-dimensional DFM by employing control volume aligned grid, also to test if EDFM performance. Figure 15 shows the tracer profiles at intermediate time of simulation for all the four fracture models. Tracer profile produced by DFM agrees with the equidimensional fracture model. The EDFM and EDFM with grids centroids aligned with fractures produce a similar tracer profile. Figure 16 shows the tracer concentration detected at the sink cell for all the four fracture cells. The behaviour of tracer via DFM follows the curve of the equidimensional fracture model. The difference is because of the higher grid resolution in the case of equidimensional fracture model. The tracer at sink for

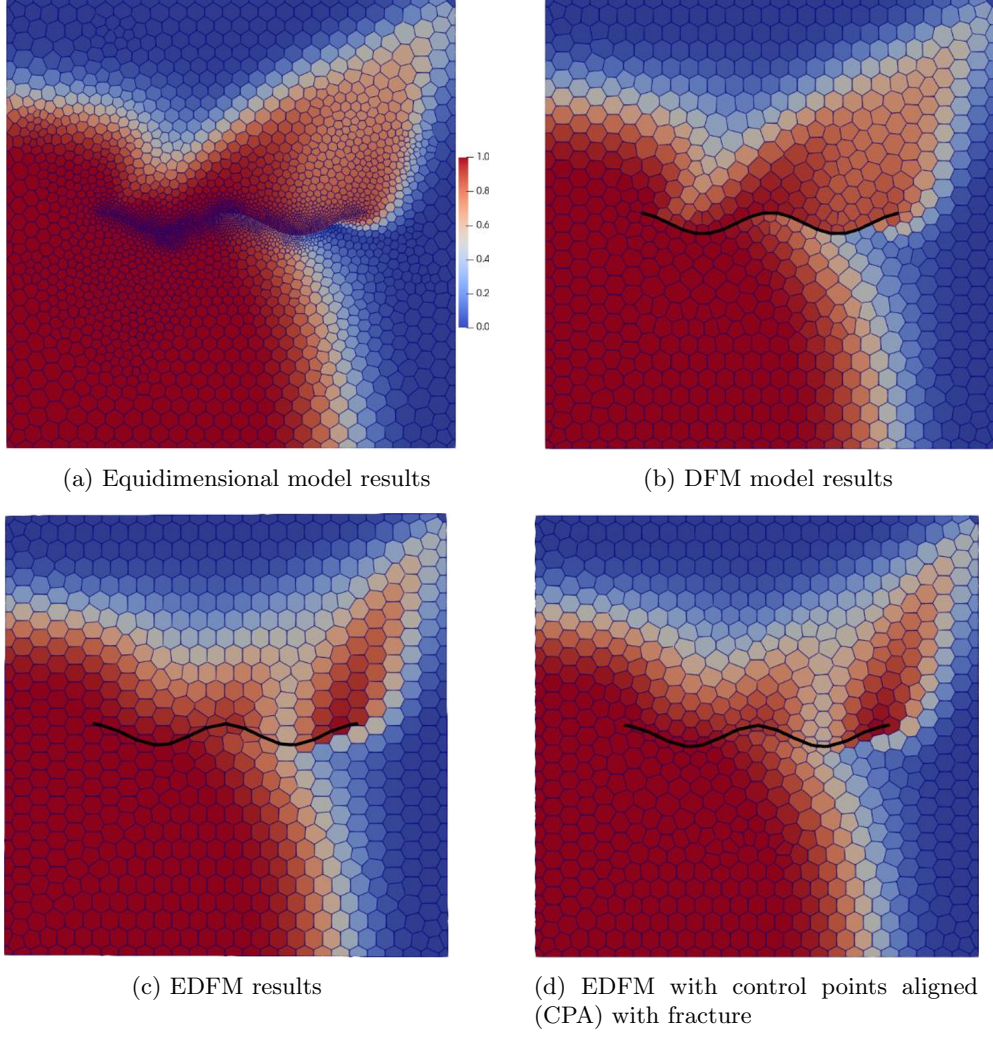


**Fig. 15:** Case-1: Tracer flow profile for test case-1 at time-step of 250

the cases of EDFM differ in behaviour when compared to the DFM because of an approximation of  $d_{NNC}$  in the fracture model. When the grid centroids are aligned with a fracture there is slight improvement in the tracer profile vs time at the sink. We also generate a grid with grid refinement in proximity to the fracture for the case of embedded discrete fracture aligned with the centroids of the grid cells. Referring to the Fig. 15(d), overall tracer profile is similar to the coarse grid result but we obtain sharp contours because of the grid refinement. The EDFM result has a difference in tracer profile around the fracture when compared to the DFM in Fig. 15. The difference is resulted because of the inherent definition of the EDFM enhanced by the geometry of the fracture. We also study EDFM with grid refinement, a close up view



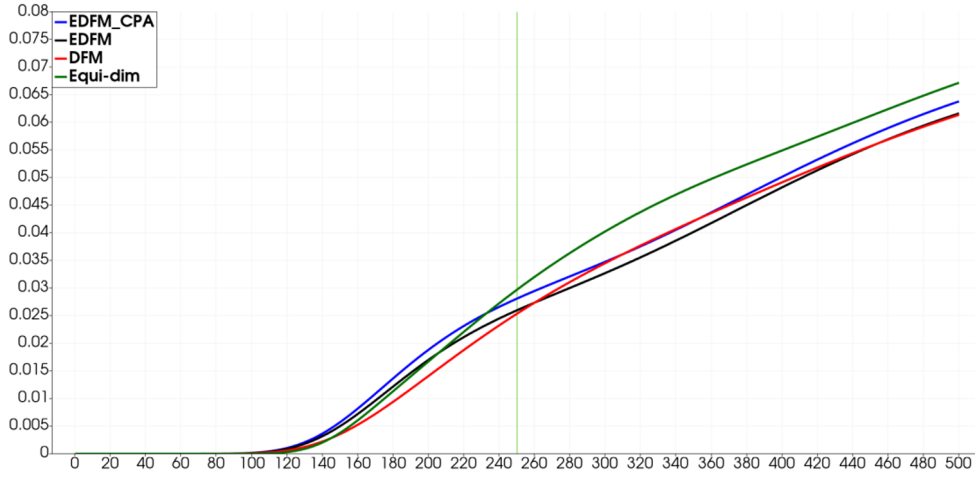


**Fig. 16:** Case-1: Tracer concentration received at the sink cell versus time. Green vertical line corresponds to the time of the tracer profiles shown above.

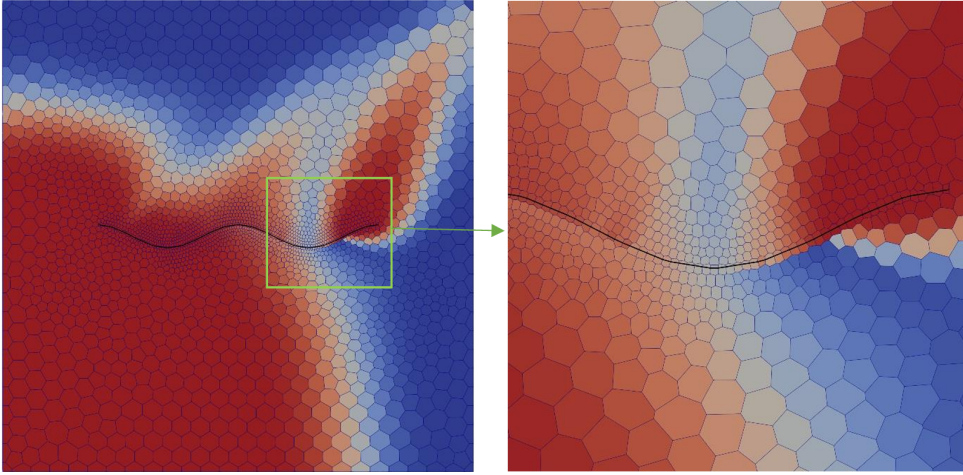


**Fig. 17:** Case-1: Tracer flow profile for the EDFM with control point aligned with fracture and matrix grid refinement around fracture at a time-step of 250. A close up view of the flow is also shown at the right.

in the Fig. 17 shows the grid resolution and the corresponding tracer profile around the fracture. The grid refinement in proximity to the fracture does not help EDFM for this case with a sinusoidal fracture.

## 4.2 Case 2a: Fracture and barrier

Next, we test a case with a permeable fracture and a barrier as illustrated in Fig.18. The pressure and tracer assignments are the same as the case-1. The barrier is assigned

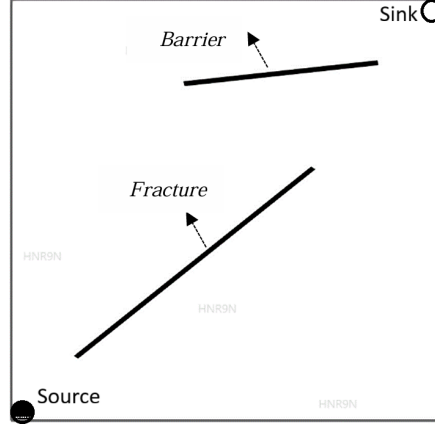


**Fig. 18:** Case-2: A model with a permeable fracture and a barrier.

with a low permeability and flow hindrance is expected because of the barrier. We discretise the domain with the PEBI cells for: a) DFM model with grid edges (lower dimensional objects) aligned with the fractures; b) EDFM where fracture overlaps the grid cells; and c) EDFM but grid centroids aligned with fracture. Figure 19 shows the tracer profiles for the three fracture models at a time step for the fracture-barrier case. It is clearly shown that EDFM does not show hindrance to the flow by the barrier when compared to the DFM which can model the barrier with physical consistency. Figure 20 shows the tracer concentration received at the sink which shows that EDFM favour higher tracer flow when compared to the DFM where flow is hindered by a barrier. The concentration of tracer increases as the fluid flows around the barrier. Similarly to the case-1, we also generate a grid for EDFM with local refinement, one with refinement around the barrier only, and the second with refinement around both the fracture and barrier where control points of PEBI grid are aligned with fracture and barrier. Figure 21 presents the tracer profile result over the two grids with two different local refinement. The barrier cannot be captured by the EDFM even though the grid has local refinement around the barrier. The refinement around the fracture presents better flow resolution comparable to the DFM in Fig.19 for this case where fracture aligns with the flow direction.

## 4.3 Case 2b: Improved EDFM

Next, we present results obtained with the improved EDFM formulation. We evaluated EDFM on both advanced control-point-aligned grids and locally refined PEBI grids. Although grid refinements and/or alignments yield some enhancement in flow

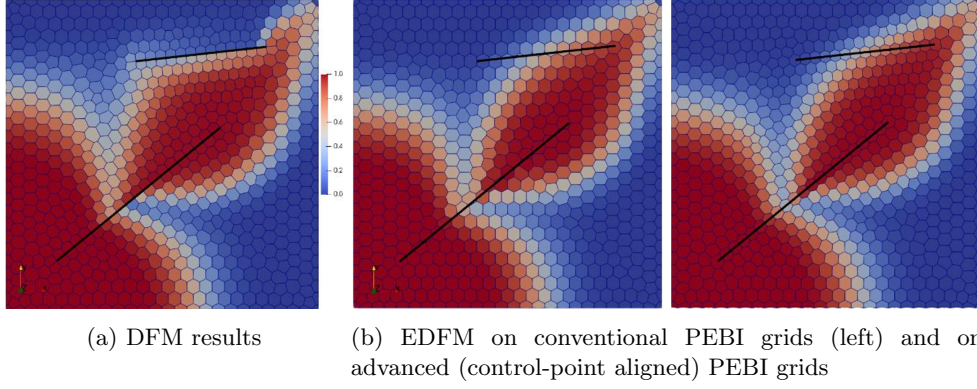


**Fig. 19:** Case-2: Comparative tracer flow profile for different fracture modelling techniques at a time-step of 250.

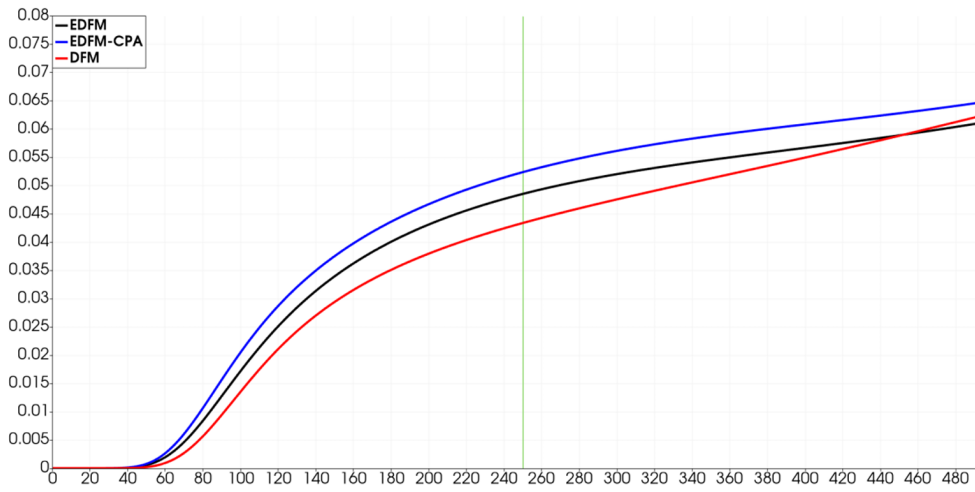


**Fig. 20:** Case-2: Tracer concentration received at the sink cell versus time. Green vertical line corresponds to the time of the tracer profiles shown above.

resolution, EDFM still fails to accurately capture the flow behavior around impermeable or low-permeability barriers, as illustrated in Fig. 21. This limitation arises because EDFM does not explicitly enforce flux continuity across fracture or barrier interfaces; instead, it relies on non-neighbouring connections (NNCs) that approximate the impact of fractures or barriers in an averaged sense. Consequently, sharp pressure gradients and localized flow deflections near barriers are not properly represented. To address this well-known shortcoming, we propose a simple but effective modification tailored for cases involving barriers. Specifically, we assign the harmonic mean of the matrix and barrier permeabilities to the matrix cells associated with the corresponding NNCs. By embedding the barrier's low permeability directly into

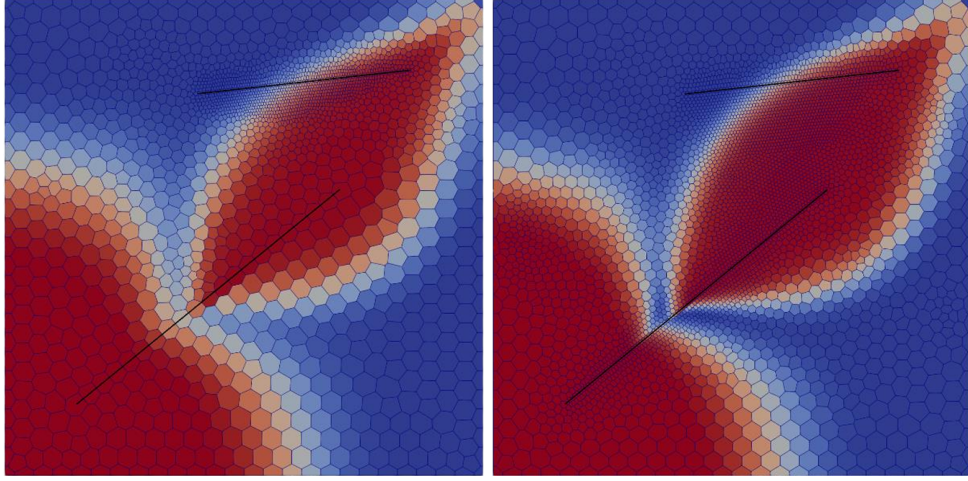


**Fig. 21:** Case-2: Tracer flow profile for the EDFM with control point aligned grid and matrix grid refinement around the barrier (left) and around both fracture and barrier (right) at a time-step of 250.

the intersected matrix cells, the NNC transmissibilities more accurately reflect the restricted flow pathways. As a result, the simulated flow field exhibits behavior consistent with that obtained using DFM, including more realistic pressure drops and flow diversion around the barrier, as demonstrated in Fig. 22. This modification significantly improves EDFM performance for barrier cases while preserving its flexibility.

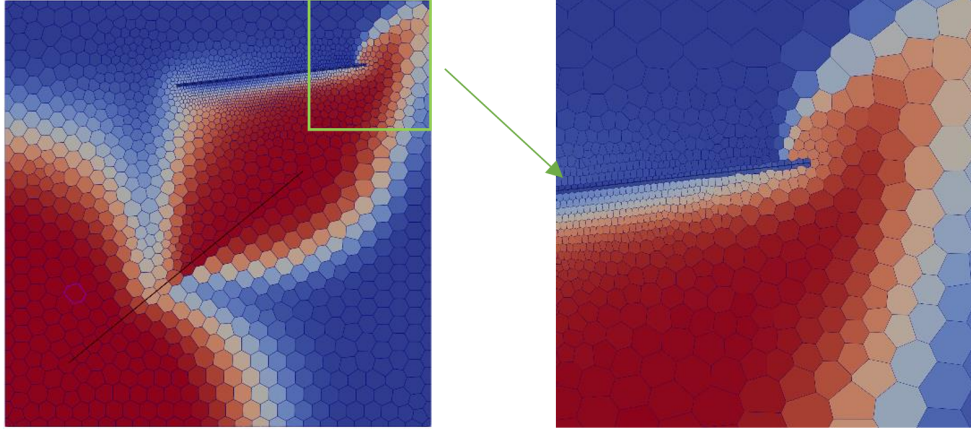


**Fig. 22:** Case-2: Tracer flow profile for improved EDFM with matrix cells perm including the effect of embedded barrier perm at a time-step of 250. A close-up view is also shown at the right.

## 5 Conclusions

PEBI grids are dual of Delaunay triangulation and are generated by employing primal (triangle/quads) as grid elements. Geological objects are discretized by employing one dimensional meshing which involves curve modelling performed with B-Spline followed by curve meshing generating segments of unit metric length. Using PEBI meshes, comparative performance and gridding requirements of three different types of fracture modelling techniques have been assessed. Equidimensional fracture modelling, employs fracture control volumes of same dimension as that of matrix. From grid generation view point, fracture (dual) cells centroids are aligned to fracture geometry. This is achieved by meshing fractures data set using Delaunay criterion coupled with feature recovery technique. Once fractures are meshed, when performing field meshing and/or applying mesh-cosmetics fracture segments integrity is ensured by protecting them with protection circles. In the equidimensional model, fracture control-volumes size is dictated by fracture aperture which not only limits the time step size but can also increases condition number of the global linear system. Equidimensional fracture modelling comes with significant added computational cost, and is not a practical approach. Lower dimensional DFM and EDFM techniques both employ lower dimensional control-volumes for fractures. Lower dimensional DFM requires PEBI cells interfaces be aligned to fracture geometry. Method presented here to generate boundary aligned PEBI grids requires halo construction performed in primal grid thereby protecting fractures as medial line of the halo cells. In contrast, EDFM does not involve any protection circle/layer, instead requires to compute fractures and PEBI cells intersection. In EDFM fractures are embedded, not aligned with PEBI grid, and non-neighbour connection(s) is established between fracture and underlying PEBI cell(s). When compared to equidimensional fracture modelling, lower dimensional fracture modelling has sound mathematical basis, whereas EDFM does not enforce flux continuity and uses non-neighbour connections to model overall effect of fractures. Test cases shows that EDFM is unable to resolve flow field across the barriers. In order to make a fair comparison between DFM (lower-dimensional) and EDFM, we test EDFM on control-point aligned PEBI grids, and slight improvements were observed. In EDFM, control-point fracture-aligned PEBI grids can improve  $d_{NNC}$  calculations. We also test EDFM performance by employing local grid refinements. For EDFM simulations, no improvements were observed with grid refinements. Numerical experiment demonstrates that in case of barrier, if permeability of underlying matrix cells includes the effect of the barrier, then EDFM can resolve flow field around the barriers, similar to that of DFM.

## References

- [1] Reiss, L.H.: The Reservoir Engineering Aspects of Fractured Formations, Illustrated edn. Editions Technip, Paris (1980)
- [2] Erhel, J., Dreuzy, J.-R.D., Poirriez, B.: Flow simulation in three-dimensional discrete fracture networks. *SIAM J. Sci. Comput.* **31**(04), 2688–2705 (2009)

- [3] Berkowitz, B.: Characterizing flow and transport in fractured geological media: A review. *Adv. Water Resour.* **25**, 861–884 (2002)
- [4] Monteagudo, J.E.P., Firoozabadi, A.: Control-volume method for numerical simulation of two-phase immiscible flow in two- and three-dimensional discrete-fractured media. *Water Resour. Res.* **40**(07), 074051–0740520 (2004)
- [5] Matthäi, S.K., Mezentsev, A., Belayneh, M.: Control-volume finite-element two-phase flow experiments with fractured rock represented by unstructured 3D hybrid meshes. In: *SPE Reservoir Simulation Symposium*. SPE, ??? (2005). Society of Petroleum Engineers
- [6] Hoteit, H., Firoozabadi, A.: An efficient numerical model for incompressible two-phase flow in fractured media. *Adv. Water Resour.* **31**(06), 891–905 (2008)
- [7] Arbogast, T., Juntunen, M., Pool, J., Wheeler, M.F.: A discontinuous galerkin method for two-phase flow in a porous medium enforcing  $h(\text{div})$  velocity and continuous capillary pressure. *Comput. Geosci.* **17**(6), 1055–1078 (2013)
- [8] Barenblatt, G., Zheltov, Y., Kochina, I.: Basic concepts in the theory of seepage of homogeneous fluids in fissurized rocks. *PMM(Soviet Appl. Math. Mech.)* **24**(05), 852–864 (1960)
- [9] Warren, J., Root, P.: The behavior of naturally fractured reservoirs. *SPE J.* **03**(03), 245–255 (1963)
- [10] Kazemi, H., Merrill, L.S., Porterfield, K.L., Zeman, P.R.: Numerical simulation of water-oil flow in naturally fractured reservoirs. *SPE J.* **16**(06), 317–326 (1976)
- [11] Gilman, J.R.: Practical aspects of simulation of fractured reservoirs. In: *International Forum on Reservoir Simulation*, Buhl, Baden-Baden, Germany (2003)
- [12] Chen, Z., Huan, G., Ma, Y.: *Computational Methods for Multiphase Flows in Porous Media*. Computational Science and Engineering. SIAM, Philadelphia (2006)
- [13] Noorishad, J., Mehran, M.: An upstream finite element method for solution of transient transport equation in fractured porous media. *Water Resour. Res.* **18**(03), 588–596 (1982)
- [14] Baca, R., Arnett, R., Langford, D.: Modeling fluid flow in fractured porous rock masses by finite element techniques. *Int. J. Numer. Methods Fluids* **04**(04), 337–348 (1984)
- [15] Lough, M.F., Lee, S.H., Kamath, J.: An efficient boundary integral formulation for flow through fractured porous media. *J. Comput. Phys.* **143**(2), 462–483 (1998)
- [16] Lee, S.H., Lough, M.F., Jensen, C.L.: Hierarchical modeling of flow in naturally



- fractured formations with multiple length scales. *Water Resour. Res.* **37**(03), 443–455 (2001)
- [17] Karimi-Fard, M., Firoozabadi, A.: Numerical simulation of water injection in fractured media using the discrete-fracture model and the Galerkin method. *SPE Reserv. Eval. Eng.* **6**(02), 117–126 (2003)
  - [18] Karimi-Fard, M., Durlofsky, L.J., Aziz, K.: An efficient discrete-fracture model applicable for general-purpose reservoir simulators. *SPE J.* **09**(02), 227–236 (2004)
  - [19] Martin, V., Jaffré, J., Roberts, J.E.: Modelling fractures and barriers as interfaces for flow in porous media. *SIAM J. Sci. Comput.* **26**, 1667–1691 (2005)
  - [20] Reichenberger, V., Jakobs, H., Bastian, P., Helmig, R.: A mixed-dimensional finite volume method for two-phase flow in fractured porous media. *Adv. Water Resour.* **29**(07), 1020–1036 (2006)
  - [21] Matthäi, S.K., Mezentsev, A., Belayneh, M.: Finite-element node-centered finite-volume experiments with fractured rock represented by unstructured hybrid element meshes. *SPE Reserv. Evalu. Eng.* **10**(6), 740–756 (2007)
  - [22] Paluszny, A., Matthäi, S.K., Hohmeyer, M.: Hybrid finite element–finite volume discretization of complex geologic structures and a new simulation workflow demonstrated on fractured rocks. *Geofluids* **7**(2), 186–208 (2007)
  - [23] Hajibeygi, H., Karvounis, D., Jenny, P.: A hierarchical fracture model for the iterative multiscale finite-volume method. *J. Comput. Phys.* **230**(24), 8729–8743 (2011)
  - [24] Girault, V., Wheeler, M.F., Ganis, B., Mear, M.E.: A lubrication fracture model in a poro-elastic medium. *Math. Models Methods Appl. Sci.* **25**(04), 587–645 (2015)
  - [25] Ahmed, R., Edwards, M.G., Lamine, S., Huisman, B.A.H., Pal, M.: Control-volume distributed multi-point flux approximation coupled with a lower-dimensional fracture model. *J. Comput. Phys.* **284**, 462–489 (2015)
  - [26] Ahmed, R., Edwards, M.G., Lamine, S., Huisman, B.A.H., Pal, M.: Three-dimensional control-volume distributed multi-point flux approximation coupled with a lower-dimensional surface fracture model. *J. Comput. Phys.* **303**, 470–497 (2015)
  - [27] Hægland, H., Assteerawatt, A., Dahle, H.K., Eigestad, G.T., Helmig, R.: Comparison of cell- and vertex-centered discretization methods for flow in a two-dimensional discrete-fracture-matrix system. *Adv. Water Resour.* **32**(12), 1740–1755 (2009)

- [28] Sandve, T.H., Berre, I., Nordbotten, J.M.: An efficient multi-point flux approximation method for discrete fracture-matrix simulations. *J. Comput. Phys.* **231**(09), 3784–3800 (2012)
- [29] Mallison, B.T., Hui, M.H., Narr, W.: Practical gridding algorithms for discrete fracture modeling workflows. In: 12th European Conference on the Mathematics of Oil Recovery. EAGE, ??? (2010)
- [30] Mustapha, H., Dimitrakopoulos, R., Graf, T., Firoozabadi, A.: An efficient method for discretizing 3D fractured media for subsurface flow and transport simulations. *Int. J. Numer. Methods Fluids* **67**(5), 651–670 (2011)
- [31] Hajibeygi, H.: Iterative multiscale finite volume method for multiphase flow in porous media with complex physics. PhD thesis, ETH Zurich (2011)
- [32] Unsal, E., Matthäi, S.K., Blunt, M.J.: Simulation of multiphase flow in fractured reservoirs using a fracture-only model with transfer functions. *Comput. Geosci.* **14**, 527–538 (2010)
- [33] Li, L., Lee, S.H.: Efficient field-scale simulation of black oil in naturally fractured reservoir through discrete fracture networks and homogenized media. *SPE Reserv. Eval. Eng.* **11**(04), 750–758 (2008)
- [34] Moinfar, A., Varavei, A., Sepehrnoori, K., Johns, R.T.: Development of an efficient embedded discrete fracture model for 3d compositional reservoir simulation in fractured reservoirs. *SPE J.* **19**(02), 289–303 (2013)
- [35] Moinfar, A., Narr, W., Hui, M.-H., Mallison, B., Lee, S.H.: Comparison of discrete-fracture and dual-permeability models for multiphase flow in naturally fractured reservoirs. In: SPE Reservoir Simulation Conference, p. 142295 (2011). SPE
- [36] Manzoor, S., Edwards, M.G., Dogru, A.H., Al-Shaalan, T.M.: Interior boundary-aligned unstructured grid generation and cell-centered versus vertex-centered cvd-mpfa performance. *Comput. Geosci.* **22**(1), 195–230 (2018)
- [37] Sahimi, M., Darvishi, R., Haghighi, M., Rasaei, M.R.: Upscaled unstructured computational grids for efficient simulation of flow in fractured porous media. *Transp. Porous Media* **83**(1), 195–218 (2010)
- [38] Fung, L.S., Ding, X.Y., Dogru, A.H.: An unstructured gridding method for densely-spaced complex wells in full-field reservoir simulation. In: SPE Reservoir Simulation Conference, p. 163648 (2013). SPE
- [39] Merland, R., Lévy, B., Caumon, G., Marschallinger, R., Zolb, R.: Building pebi grids conforming to 3d geological features using centroidal voronoi tessellations. IAMG Proceedings (2011)



- [40] Palagi, C.L., Aziz, K.: Use of voronoi grid in reservoir simulation. SPE Advanced Technology Series **2**(02), 69–77 (1994)
- [41] Palagi, C.L., Aziz, K.: Use of voronoi grid in reservoir simulation. Society of Petroleum Engineers **2**(2), 69–77 (2007)
- [42] Frey, P.J., Borouchaki, H., George, P.-L.: 3d delaunay mesh generation coupled with an advancing-front approach. Comput. Methods Appl. Mech. Eng. **157**(1-2), 115–131 (1998)
- [43] Manzoor, S., Edwards, M., Dogru, A.: Acute boundary aligned unstructured grid generation and consistent flux approximations. In: ECMOR XVI-16th European Conference on the Mathematics of Oil Recovery, vol. 2018, pp. 1–24 (2018). European Association of Geoscientists & Engineers
- [44] De Boor, C.: On calculating with b-splines. J. Approximation Theory **6**(1), 50–62 (1972)
- [45] Green, P.J., Sibson, R.: Computing dirichlet tessellations in the plane. The comput. J. **21**(2), 168–173 (1978)
- [46] Weatherill, N.P.: Delaunay triangulation in computational fluid dynamics. Comput. Math. Appl. **24**(5-6), 129–150 (1992)
- [47] Sloan, S.W.: A fast algorithm for generating constrained delaunay triangulations. Comput. & Struc. **47**(3), 441–450 (1993)
- [48] Lawson, C.L.: Properties of n-dimensional triangulations. Comput. Aided Geom. Des. **3**(4), 231–246 (1986)
- [49] Sibson, R.: Locally equiangular triangulations. The computer J. **21**(3), 243–245 (1978)
- [50] Hassan, O., Probert, E., Morgan, K., Weatherill, N.: Unsteady flow simulation using unstructured meshes. Comput. Methods Appl. Mech. Eng. **189**(4), 1247–1275 (2000)
- [51] Rebay, S.: Efficient unstructured mesh generation by means of delaunay triangulation and bowyer-watson algorithm. J. Comput. Phys. **106**(1), 125–138 (1993)
- [52] George, P.-L., Borouchaki, H.: Delaunay Triangulation and Meshing: Application to Finite Elements. Hermès science, ??? (1998)
- [53] Sazonov, I., Wang, D., Hassan, O., Morgan, K., Weatherill, N.: A stitching method for the generation of unstructured meshes for use with co-volume solution techniques. Comput. Methods Appl. Mech. Eng. **195**(13-16), 1826–1845 (2006)

- [54] Marcum, D.L., Weatherill, N.P.: Unstructured grid generation using iterative point insertion and local reconnection. *AIAA journal* **33**(9), 1619–1625 (1995)
- [55] Mavriplis, D.J.: An advancing front delaunay triangulation algorithm designed for robustness. *J. Comput. Phys.* **117**(1), 90–101 (1995)
- [56] Müller, J.-D., Roe, P.L., Deconinck, H.: A frontal approach for internal node generation in delaunay triangulations. *Int. J. Numer. Methods Fluids* **17**(3), 241–255 (1993)
- [57] Aziz, K., Settari, A.: *Petroleum Reservoir Simulation*. Elsevier Applied Science Publishers, ??? (1986). Chap. 5
- [58] Kocabas, I., Maier, F.: Analytical and numerical modeling of tracer flow in oil reservoirs containing high permeability streaks. In: *SPE Middle East Oil and Gas Show and Conference*, p. 164330 (2013). SPE
- [59] Wong, D., Doster, F., Geiger, S.: Embedded discrete fracture models. In: Lie, K.-A., Møyner, O. (eds.) *Advanced Modeling with the MATLAB Reservoir Simulation Toolbox*, pp. 375–408. Cambridge University Press, Cambridge (2021)